Electron *g* factors and optical properties of InAs quantum ellipsoids

2006 J. Phys.: Condens. Matter 18 4945

(http://iopscience.iop.org/0953-8984/18/20/018)

INSTITUTE OF PHYSICS PUBLISHING JOURNAL OF PHYSICS: CONDENSED MATTER

J. Phys.: Condens. Matter **18** (2006) 4945–4954 doi:10.1088/0953-8984/18/20/018

Electron *g* factors and optical properties of InAs quantum ellipsoids

X W Zhang, Y H Zhu and J B Xia

Chinese Center of Advanced Science and Technology (World Laboratory), PO Box 8730, Beijing 100080, People's Republic of China
and
Institute of Semiconductors, Chinese Academy of Sciences, PO Box 912, Beijing 100083, People's Republic of China

Received 21 December 2005, in final form 16 March 2006
Published 5 May 2006
Online at stacks.iop.org/JPhysCM/18/4945

Abstract

The electronic structure, electron *g* factors and optical properties of InAs quantum ellipsoids are investigated, in the framework of the eight-band effective-mass approximation. It is found that the light-hole states come down in comparison with the heavy-hole states when the spheres are elongated, and become the lowest states of the valence band. Circularly polarized emissions under circularly polarized excitations may have opposite polarization factors to the exciting light. For InAs ellipsoids the length, which is smaller than 35 nm, is still in a strongly quantum-confined regime. The electron *g* factors of InAs spheres decrease with increasing radius, and are nearly 2 when the radius is very small. The quantization of the electron states quenches the orbital angular momentum of the states. Actually, as some of the three dimensions increase, the electron *g* factors decrease. As more dimensions increase, the *g* factors decrease more. The dimensions perpendicular to the direction of the magnetic field affect the *g* factors more than the other dimension. The magnetic field along the *z* axis of the crystal structure causes linearly polarized emissions in the spheres, which emit unpolarized light in the absence of magnetic field.

1. Introduction

Narrow-gap semiconductors have long been discussed for their special characteristics. These give rise to a lot of interesting physical effects, as well as useful technological applications, such as infrared detectors and lasers.

For wide use in applications, people are paying more and more attention to the narrow-gap semiconductors. Regarded as the typical example, lots of investigations on InAs quantum dots have been reported in recent decades. InAs quantum dots have been synthesized by colloidal chemistry techniques [1], or epitaxial growth techniques [2]. Short quantum rods were also synthesized which have ellipsoidal shape as shown in the TEM images [3]. Using

the same method, other quantum ellipsoids were also synthesized [4–6], whose shape can be controlled [7–10]. Linearly polarized emissions from InAs ellipsoids in the absence of magnetic field were observed [3]. Circularly polarized emissions under circularly polarized excitations were measured [11, 12]. Electron g factors of these low-dimensional systems were investigated experimentally [13, 14] and theoretically [15]. The electronic structure has been calculated using the effective-mass model [16, 17], the pseudopotential method [18, 19] or the empirical tight-binding description [20].

In this paper, we investigate the electronic structure, electron g factors and optical properties of InAs quantum ellipsoids, in the framework of the eight-band effective-mass approximation, in the presence of external homogeneous magnetic field. We have already studied the electronic structure and optical properties under magnetic field of CdSe quantum dots in the framework of the six-band effective-mass approximation [21]. Now, we extend the former model to this eight-band and ellipsoid case. The remainder of this paper is organized as follows. In section 2 we give the form of the Hamiltonian. Our numerical results and discussions are given in section 3. Finally, we draw a brief conclusion in section 4.

2. Theory model and calculations

The eight-band effective-mass Hamiltonian for the zinc-blende semiconductors with $\mathbf{k}\cdot\mathbf{p}$ perturbation method at Γ point of the Brillouin zone has been derived previously [22]. Neglecting the spin–orbit coupling, the Hamiltonian is represented in the following form for the Bloch basic functions of $|S\rangle$, $|11\rangle = (X+\mathrm{i}Y)/\sqrt{2}$, $|10\rangle = Z$ and $|1-1\rangle = (X-\mathrm{i}Y)/\sqrt{2}$,

$$H_{\mathrm{int}} = \frac{1}{2m_0}\begin{pmatrix} \epsilon_{\mathrm{g}}+P_{\mathrm{e}} & -\mathrm{i}p_0P_1^{(1)} & \mathrm{i}p_0P_0^{(1)} & \mathrm{i}p_0P_{-1}^{(1)} \\ -\mathrm{i}p_0P_{-1}^{(1)} & -P_{\mathrm{l}} & -S & -T \\ -\mathrm{i}p_0P_0^{(1)} & -S^{\star} & -P_3 & -S \\ \mathrm{i}p_0P_1^{(1)} & -T^{\star} & -S^{\star} & -P_{\mathrm{l}} \end{pmatrix} \tag{1}$$

where

$$P_{\mathrm{e}} = \alpha_1 p^2 - \sqrt{\tfrac{2}{3}}\alpha_2 P_0^{(2)}, \tag{2a}$$

$$P_{\mathrm{l}} = \gamma_{1h} p^2 - \sqrt{\tfrac{2}{3}}\gamma_2 P_0^{(2)}, \tag{2b}$$

$$P_3 = \gamma_1' p^2 + 2\sqrt{\tfrac{2}{3}}\gamma_2' P_0^{(2)}, \tag{2c}$$

$$T = \eta P_{-2}^{(2)} + \delta P_2^{(2)}, \tag{2d}$$

$$T^* = \eta P_2^{(2)} + \delta P_{-2}^{(2)}, \tag{2e}$$

$$S = \sqrt{2}\gamma_3' P_{-1}^{(2)}, \tag{2f}$$

$$S^* = -\sqrt{2}\gamma_3' P_1^{(2)}. \tag{2g}$$

$P^{(1)}$ and $P^{(2)}$ are the first-order and second-order irreducible tensors of the momentum operator, respectively. $\epsilon_{\mathrm{g}} = 2m_0E_{\mathrm{g}}$, and E_{g} is the bandgap of bulk material. $p_0 = \sqrt{2m_0E_{\mathrm{p}}}$, and E_{p} is the matrix element of Kane's theory.

As we know, the Luttinger parameters γ_2^L and γ_3^L reflect the asymmetry resulting from the corrugation of the hole constant-energy surface connected with zinc-blende symmetry of the crystal lattice. If we take $\gamma^L = (2\gamma_2^L + 3\gamma_3^L)/5$, the energy levels obtained in the spherical potential are correct to the first order of perturbation theory for the $\Delta\gamma^L = \gamma_3^L - \gamma_2^L$ [23]. The second order correction is usually small because $\gamma_3^L - \gamma_2^L \ll \gamma_2^L + \gamma_3^L$. Therefore afterwards we take $\gamma_2^L = \gamma_3^L = \gamma^L$.

As we have take into account the coupling of the valence band and the conduction band, the Luttinger parameters γ_1^L, γ^L should subtract the contribution from the conduction band, $\gamma_1 = \gamma_1^L - E_p/3E_g$, $\gamma = \gamma^L - E_p/6E_g$ [24]. The electron effective mass should subtract the contribution from the valence band. The inverse of the electron effective mass m_c at the bottom of the conduction band includes the contribution from the valence band and the remaining one which is denoted by the parameter α, using the relation as [25]:

$$\frac{1}{m_c} = \frac{1}{m_0}\left(\frac{E_p}{3}\left[\frac{2}{E_g} + \frac{1}{E_g + \Delta_{so}}\right] + \alpha\right). \tag{3}$$

For zinc-blende quantum spheres, the effective-mass parameters in equation (1) are

$$\alpha_1 = \alpha, \qquad \alpha_2 = 0, \tag{4a}$$

$$\gamma_{1h} = \gamma_1' = \gamma_1, \tag{4b}$$

$$\gamma_2 = \gamma_2' = \gamma_3' = \gamma, \tag{4c}$$

$$\eta = 2\gamma, \qquad \delta = 0. \tag{4d}$$

Taking the spin–orbit coupling into account, we represent the eight-band effective-mass Hamiltonian in Bloch function bases $|S\rangle\uparrow$, $|11\rangle\uparrow$, $|10\rangle\uparrow$, $|1-1\rangle\uparrow$, $|S\rangle\downarrow$, $|11\rangle\downarrow$, $|10\rangle\downarrow$, $|1-1\rangle\downarrow$ as

$$H_{eb} = \begin{pmatrix} H_{int} & \\ & H_{int} \end{pmatrix} - H_{so}. \tag{5}$$

The spin–orbit coupling Hamiltonian H_{so} has the form of

$$H_{so} = \begin{pmatrix} 0 & 0 & 0 & 0 & 0 & 0 & 0 & 0 \\ 0 & 0 & 0 & 0 & 0 & 0 & 0 & 0 \\ 0 & 0 & \lambda & 0 & 0 & \sqrt{2}\lambda & 0 & 0 \\ 0 & 0 & 0 & 2\lambda & 0 & 0 & -\sqrt{2}\lambda & 0 \\ 0 & 0 & 0 & 0 & 0 & 0 & 0 & 0 \\ 0 & 0 & \sqrt{2}\lambda & 0 & 0 & 2\lambda & 0 & 0 \\ 0 & 0 & 0 & -\sqrt{2}\lambda & 0 & 0 & \lambda & 0 \\ 0 & 0 & 0 & 0 & 0 & 0 & 0 & 0 \end{pmatrix}, \tag{6}$$

where

$$\lambda = \frac{\hbar^3}{4m_0^2c^2}\langle X|\frac{\partial V}{\partial x}\frac{\partial}{\partial y}|Y\rangle = \frac{\Delta_{so}}{3}. \tag{7}$$

Δ_{so} is the spin–orbital splitting energy of the valence band.

We assume that the electrons and holes are confined in a infinitely high potential barrier, so that the wavefunctions at the boundary are zero. The envelope function including the electron and hole states is expanded with the spherical Bessel functions and spherical harmonic functions as

$$\Psi = \sum_m \sum_{l,n} \begin{pmatrix} e_{l,n,\uparrow}^{(m)} A_{l,n} j_l(K_n^l r) Y_{l,m} \\ a_{l,n,\uparrow}^{(m-1)} A_{l,n} j_l(K_n^l r) Y_{l,m-1} \\ b_{l,n,\uparrow}^{(m)} A_{l,n} j_l(K_n^l r) Y_{l,m} \\ c_{l,n,\uparrow}^{(m+1)} A_{l,n} j_l(K_n^l r) Y_{l,m+1} \\ e_{l,n,\downarrow}^{(m+1)} A_{l,n} j_l(K_n^l r) Y_{l,m+1} \\ a_{l,n,\downarrow}^{(m)} A_{l,n} j_l(K_n^l r) Y_{l,m} \\ b_{l,n,\downarrow}^{(m+1)} A_{l,n} j_l(K_n^l r) Y_{l,m+1} \\ c_{l,n,\downarrow}^{(m+2)} A_{l,n} j_l(K_n^l r) Y_{l,m+2} \end{pmatrix}, \tag{8}$$

where $\alpha_n^l = K_n^l R$ is the nth zero point of $j_l(x)$, R is the radius of the quantum spheres, and A_{ln} is the normalization constant,

$$A_{ln} = \sqrt{\frac{2}{R^3}} \frac{1}{j_{l+1}(\alpha_n^l)}. \tag{9}$$

For simplicity, hereafter we assume that the external magnetic field is applied along the z axis or x axis of the crystal structure. We can choose the symmetric gauge, so that the vector potential is written as

$$\mathbf{A} = (-\tfrac{1}{2}B_z y, \tfrac{1}{2}B_z x - \tfrac{1}{2}B_x z, \tfrac{1}{2}B_x y). \tag{10}$$

In the presence of external magnetic field, the momentum operator changes into $\mathbf{p} \Rightarrow \mathbf{p} + e\mathbf{A}$. We can divide the whole Hamiltonian into

$$H = H_{\text{eb}} + H_{\text{asym}}^a + H_{\text{Zeeman}} + H_{\text{mm}}, \tag{11}$$

where

$$H_{\text{asym}}^a = \begin{pmatrix} 0 & & & \\ & H_{\text{asym}} & & \\ & & 0 & \\ & & & H_{\text{asym}} \end{pmatrix}. \tag{12}$$

H_{asym} has been given in detail before [21, 26]. H_{Zeeman} is the spin-Zeeman-splitting Hamiltonian. H_{mm} is the remainder term, which is similar to the magnetic-momentum Hamiltonian given by Zhang *et al* [21].

For quantum ellipsoids, we introduce a coordinate transformation as [27]

$$x = x', \tag{13a}$$

$$y = y', \tag{13b}$$

$$z = ez', \tag{13c}$$

$$p_z = \frac{1}{e} p_z', \tag{13d}$$

where e is the aspect ratio of the ellipsoid length to diameter.

We calculate the linear polarization factor in an ellipsoidal system. We assume that the wave propagates along the y axis of the crystal structure. The linear polarization factor is calculated by

$$P = (I_z - I_x)/(I_z + I_x). \tag{14}$$

I_z and I_x are the intensities of z- and x-polarized transitions. For the optical transition between a given electron state and a given hole state, they are proportional to

$$I_z = \left\{ \sum_{l,n,m,\sigma} b_{l,n,\sigma}^{(m)} e_{l,n,\sigma}^{(m)} \right\}^2, \tag{15}$$

$$I_x = \left\{ \sum_{l,n,m,\sigma} \frac{1}{\sqrt{2}} (a_{l,n,\sigma}^{(m)} e_{l,n,\sigma}^{(m)} + c_{l,n,\sigma}^{(m)} e_{l,n,\sigma}^{(m)}) \right\}^2. \tag{16}$$

$a_{l,n,\sigma}^{(m)}$, $b_{l,n,\sigma}^{(m)}$, $c_{l,n,\sigma}^{(m)}$ and $e_{l,n,\sigma}^{(m)}$ are given in equation (8).

Considering the temperature effect, we multiply the Boltzmann distribution factor of each state, and sum up all contributions to the intensities.

Table 1. The effective-mass parameters of InAs material.

m_c	γ_1^L	γ^L	E_p (eV)	E_g (eV)	Δ_{so} (eV)
0.022 26	19.67	8.92	21.6	0.418	0.380

3. Results and discussion

In this section, we calculate the electronic structure, electron g factors and optical properties of InAs quantum ellipsoids. The effective-mass parameters [28] used in this paper are listed in table 1. However, energy band parameters measured in the bulk material include some nonlocal contributions that are absent in nanocrystals [29, 30]. The nonlocal contributions are

$$\Delta\gamma_1 = -5\delta_{nl}, \qquad \Delta\gamma = -4\delta_{nl} \tag{17}$$

$$\Delta\alpha = -10\delta_{nl}, \qquad \delta_{nl} = \frac{2}{15\pi\epsilon_r E_g}\sqrt{\frac{E_B E_p}{3}}, \tag{18}$$

where $E_B = 27.211$ eV is the Bohr energy, and $\epsilon_r = 15.15$ [28] is the dielectric constant of InAs material.

We use the energy unit,

$$\varepsilon_0 = \frac{1}{2m_0}\left(\frac{\hbar}{R}\right)^2, \tag{19}$$

and the dimensionless magnetic field strength unit,

$$b = \frac{\hbar e B}{m_0 \varepsilon_0}. \tag{20}$$

3.1. Electronic structure

The hole states of InAs ellipsoids with radius of $R = 2.0$ nm at $b = 0$ as functions of e are shown in figure 1(a). Here we take the negative hole energy as positive. The symbol of each energy level represents the main components of its wavefunction and degeneration rate. For example, $S_L(2)$ means that the states consist mainly of S ($l = 0$) light-hole states and are doubly degenerate, and $S_H(2)$ is the S heavy-hole doublet. $P_A(2)$ and $P_B(2)$ are two P ($l = 1$) doublets. They are mixed with light-hole and heavy-hole states because the $l = 1$ angular-momentum state is a triplet. We see that the S doublets and P doublets are degenerated when $e = 1$, respectively, and split when $e \neq 1$. When the ellipsoids are elongated, the Z Bloch state comes down in comparison with the X and Y Bloch states [27]; this will cause linearly polarized emissions, which have been theoretically [27] and experimentally [3] investigated. The light-hole states have many Z Bloch state components, and the heavy-hole states do not. So the $S_L(2)$ doublet comes down in comparison with the $S_H(2)$ doublet, as shown in figure 1(a). When the ellipsoids are excited by circularly polarized light which propagate along the z axis of the crystal structure, what will happen? The light-hole states are $1/\sqrt{6}(X + iY)\downarrow - \sqrt{2/3}Z\uparrow$ and $-1/\sqrt{6}(X - iY)\uparrow - \sqrt{2/3}Z\downarrow$. The heavy-hole states are $1/\sqrt{2}(X + iY)\uparrow$ and $1/\sqrt{2}(X - iY)\downarrow$. The Bloch states $X \pm iY$ contribute to the $\sigma^{\mp}$-polarized absorptions and emissions. As the proportion of $X \pm iY$ Bloch states of heavy-hole states, which is 100%, is much bigger than that of the light-hole states, the circularly polarized absorptions mainly happen in the heavy-hole states. Considering the temperature effect, because the light-hole states are the lowest states as shown in figure 1(a) when $e = 3$, the circularly polarized

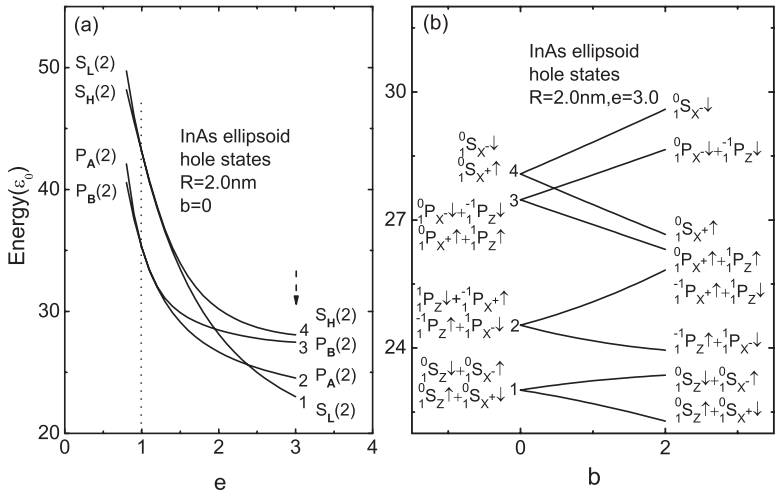

Figure 1. (a) Hole states of InAs ellipsoids with radius of $R = 2.0$ nm at $b = 0$ as functions of e. (b) Hole states of InAs ellipsoids with radius of $R = 2.0$ nm and aspect ratio $e = 3.0$ as functions of b.

emissions mainly happen in the light-hole states. Because the light-hole and heavy-hole states have opposite combination relations between $X \pm \mathrm{i}Y$ and $\uparrow\downarrow$, so the emitting light will have opposite polarization factors to the exciting light. This phenomenon has been investigated both experimentally [11, 12] and theoretically [31].

The hole states of InAs ellipsoids with radius of $R = 2.0$ nm and aspect ratio $e = 3.0$ as functions of b are shown in figure 1(b). The symbol of each energy level represents the main components of its wavefunction. For example, ${}^{0}_{1}S_{X^+}\uparrow$ means that the state consists mainly of the $n = 1$, $l = 0$, $m = 0$ state of the effective-mass envelope function multiplied by the $\frac{1}{\sqrt{2}}(X + \mathrm{i}Y)$ Bloch state of the valence-band top and the spin-up state. We see that the doublets split under magnetic field. The $S_H(2)$ doublet splits about three times wider than the $S_L(2)$ doublet, in agreement with the famous angular momentum $\pm 3/2$ and $\pm 1/2$ of the heavy hole and light hole, respectively.

The bandgap of InAs ellipsoids with radius of $R = 2.0$ nm as a function of e is shown in figure 2. We see that the bandgap decreases as e increases. Moreover, when e is as big as 8, the bandgap is still decreasing not very slowly, that means that this length is still in a strongly quantum-confined regime. This is due to the big bulk exciton Bohr radius of InAs material, which is about 35 nm. Actually, when $R = 2.0$ nm and $e = 8$, the length is 32 nm, and is still smaller than the bulk exciton Bohr radius.

3.2. Electron g-factor

The electron g factors of InAs spheres as functions of E_g are shown in figure 3(a). The bandgap of InAs spheres as a function of R is shown in figure 3(b). We see that as R increases E_g decreases, and as E_g decreases the electron g factors decrease. The dashed line is calculated from the formula

$$g = 2 - \frac{2E_p\Delta_{so}}{3E_g(E_g + \Delta_{so})}. \tag{21}$$

The solid line is calculated from our model. We see that if we elongate the solid line, which is shown by the dotted line, it will cross with the dashed line at $(0.418, -14.4)$. 0.418 eV and

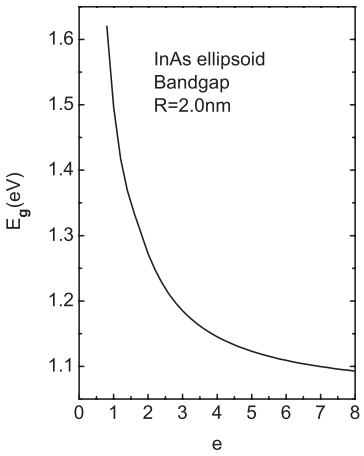

Figure 2. Bandgap of InAs ellipsoids with radius of $R = 2.0$ nm as a function of e.

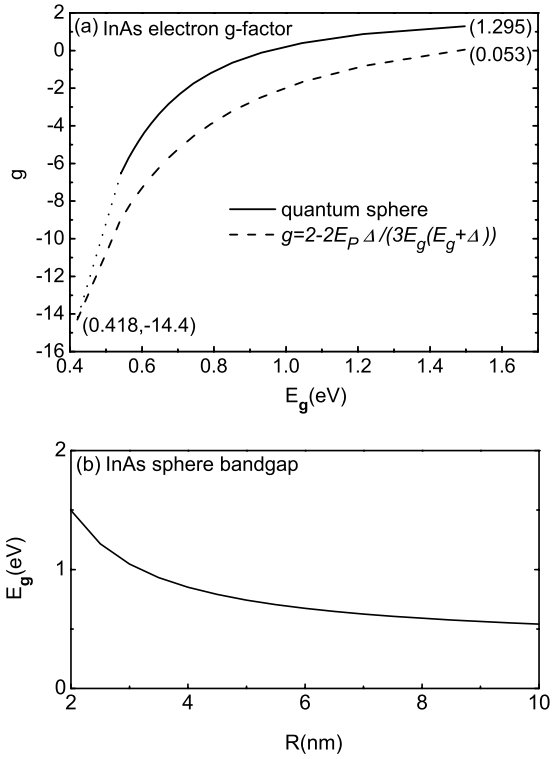

Figure 3. (a) Electron g factors of InAs spheres as functions of E_{g}. (b) Bandgap of InAs spheres as a function of R.

-14.4 are the bandgap and electron g factor of the bulk material, respectively [28]. So the two calculations coincide in the bulk material case. But in the dot case, they are very different. For example, when our result is 1.295, the formula result is 0.053. The formula result is wrong, and is rather smaller than the real case. Our calculation coincides with the calculation by

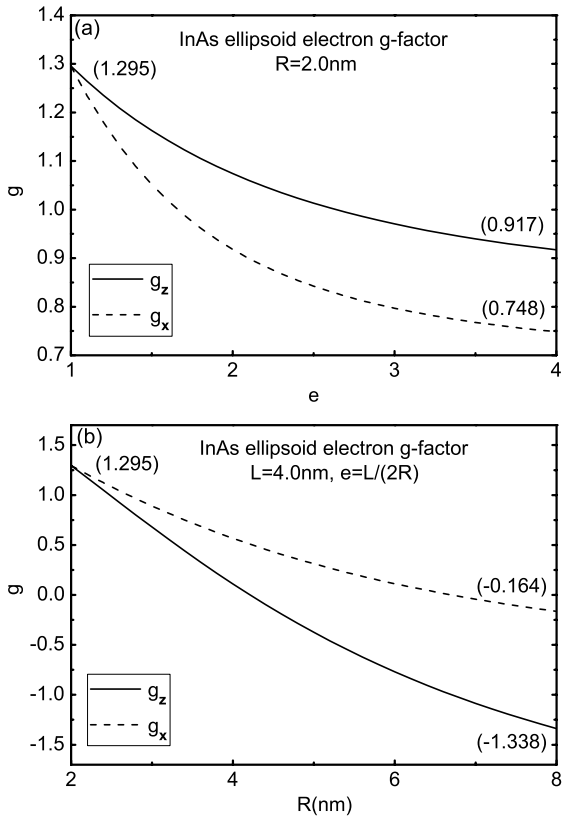

Figure 4. (a) Electron g factors of InAs ellipsoids with radius of $R = 2.0$ nm as functions of e. (b) Electron g factors of InAs ellipsoids with length of $L = 4.0$ nm as functions of R.

Flatt *et al* [15], who name this phenomenon 'orbital momentum quenching'. The quantization of the electron states quenches the orbital angular momentum of the states.

The electron g factors of InAs ellipsoids with radius of $R = 2.0$ nm as functions of e are shown in figure 4(a). We see that when $e = 1$, in the sphere case, $g_z = g_x = 1.295$. As e increases, g_z and g_x both decrease, but g_x decreases more quickly. When $e = 4$, $g_z = 0.917$ and $g_x = 0.748$. The electron g factors of InAs ellipsoids with length of $L = 4.0$ nm as functions of R are shown in figure 4(b). We see that when $R = 2$ nm, in the sphere case, $g_z = g_x$. As R increases, g_z and g_x both decrease, but g_z decreases more quickly. When $R = 8$ nm, $g_z = -1.338$, $g_x = -0.164$. Actually, in figure 3 three dimensions are increased, and in figure 4 one or two dimensions are increased. We see that when the dots are very small the electron g factors are nearly 2, and when the three dimensions are all very large the electron g factors are nearly -14.4. As the dimensions increase, the electron g factors decrease. As more dimensions increase, the electron g factors decrease more. Because one and two dimensions increase in figures 4(a) and (b), respectively, the g factors decrease more in figure 4(b) than in figure 4(a). We see that when the dimension along the z axis of the crystal structure (i.e. perpendicular to the x axis) is increased g_x decreases more (see figure 4(a)), and when the dimensions perpendicular to the z axis are increased g_z decreases more (see figure 4(b)). So the dimensions perpendicular to the direction of the magnetic field affect the g factors more than the other dimension.

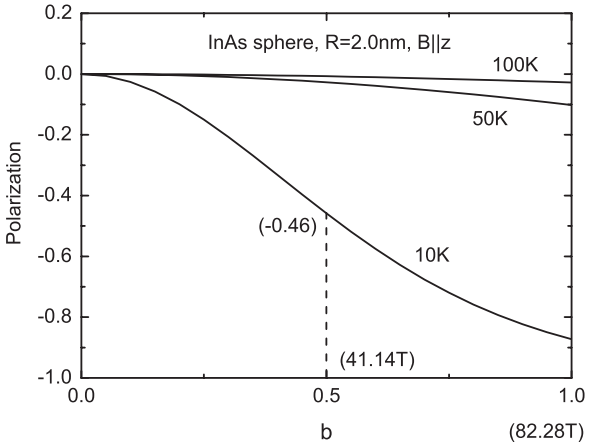

Figure 5. Linear polarization factors of InAs spheres with radius of $R = 2.0$ nm as functions of b ($B \parallel z$).

3.3. Linear polarization

The linear polarization factors of InAs spheres with radius of $R = 2.0$ nm as functions of b ($B \parallel z$) are shown in figure 5. We see that in the absence of magnetic field, the emissions are linearly unpolarized. In the presence of magnetic field along the z axis of the crystal structure, there are x-polarized emissions. As b increases, the linear polarization factors decrease. At lower temperature, the factors decrease more quickly. When $T = 10$ K and $B = 41.14$ T, the linear polarization factor is -0.46.

4. Conclusions

The electronic structure, electron g factors and optical properties of InAs quantum ellipsoids are investigated. As the spheres are elongated, the light-hole states come down in comparison with the heavy-hole states and become the lowest states of the valence band. When the light-hole states are the lowest states of the valence band, circularly polarized emissions may have opposite polarization factors to the circularly polarized exciting light. As the InAs bulk exciton Bohr radius is as big as 35 nm, InAs ellipsoids with length of 32 nm are still in a strongly quantum-confined regime [3]. The electron g factors of InAs quantum spheres decrease with increasing radius. When R is very small the g factors are nearly 2. When R is sufficiently big, the g factors are nearly -14.4, which is similar to the bulk material case. The quantization of the electron states quenches the orbital angular momentum of the states, which is in agreement with the other calculation [15]. The electron g factors are dependent on the three dimensions. Actually, as the dimensions increase, the g factors decrease. As more dimensions increase, the g factors decrease more. The dimensions perpendicular to the direction of the external magnetic field affect the g factors more than the other dimension. For example, when $2R = 4$ nm and $L = 16$ nm $g_z = 0.917$ and $g_x = 0.748$, and when $L = 4$ nm and $2R = 16$ nm $g_z = -1.338$ and $g_x = -0.164$. The magnetic field along the z axis of the crystal structure introduces x-polarized emissions in the spheres.

Acknowledgments

This work was supported by the National Natural Science Foundation Nos 90301007, 60521001 and the special funds for Major State Basic Research Project No G001CB3095 of China.

References

[1] Guzelian A, Banin U, Kadavanich A, Peng X and Alivisatos A 1996 *Appl. Phys. Lett.* **69** 1432
[2] Leonard D, Krishnamurthy M, Reaves C M, Denbaars S P and Petroff P M 1993 *Appl. Phys. Lett.* **63** 3203
[3] Kan S, Mokari T, Rothenberg E and Banin U 2003 *Nat. Mater.* **2** 155
[4] Hu J, Li L-S, Yang W, Manna L, Wang L-W and Alivisatos A P 2001 *Science* **292** 2060
[5] Peng Z and Peng X 2001 *J. Am. Chem. Soc.* **123** 1389
[6] Qu L and Peng X 2002 *J. Am. Chem. Soc.* **124** 2049
[7] Manna L, Scher E C and Alivisatos A P 2002 *J. Cluster Sci.* **13** 521
[8] Lee S-M, Cho S-N and Cheon J 2003 *Adv. Mater.* **15** 441
[9] El-Sayed M A 2004 *Acc. Chem. Res.* **37** 326
[10] Peng X 2003 *Adv. Mater.* **15** 459
[11] Cortez S, Krebs O, Laurent S, Senes M, Marie X, Voisin P, Ferreira R, Bastard G, Gerard J M and Amand T 2002 *Phys. Rev. Lett.* **89** 207401
[12] Paillard M, Marie X, Renucci P, Amand T, Jbeli A and Gerard J M 2001 *Phys. Rev. Lett.* **86** 1634
[13] Snelling M J, Flinn G P, Plaut A S, Harley R T, Tropper A C, Eccleston R and Phillips C C 1991 *Phys. Rev.* B **44** 11345
[14] Sirenko A A, Ruf T, Kurtenbach A and Eberl K 1996 *Proc. Int. Conf. on the Physics of Semiconductors (Berlin, 1996)* ed M Scheffler and R Zimmermann (Singapore: World Scientific) p 1385
[15] Pryor C E and Flatt M E 2006 *Phys. Rev. Lett.* **96** 026804
[16] Pokatilov E P, Fonoberov V A, Fomin V M and Devreese J T 2001 *Phys. Rev.* B **64** 245328
[17] Banin U, Lee J C, Guzelian A A, Kadavanich A V, Alivisatos A P, Jaskolski W, Bryant G, Efros Al L and Rosen M 1998 *J. Chem. Phys.* **109** 2306
[18] Williamson A J and Zunger A 2000 *Phys. Rev.* B **61** 1978
[19] Mizel A and Cohen M 1998 *Solid State Commun.* **104** 404
[20] Lee S, Jönsson L, Wilkins J W, Bryant G W and Klimeck G 2001 *Phys. Rev.* B **63** 195318
[21] Zhang X W and Xia J B 2005 *Phys. Rev.* B **72** 075363
[22] Kane E O 1982 *Handbook on Semiconductors* vol 1, ed W Paul and T S Moss (Amsterdam: North-Holland)
[23] Gel'mont B L and D'yakonov M I 1971 *Fiz. Tekh. Poluprovodn.* **5** 2191
Gel'mont B L and D'yakonov M I 1972 *Sov. Phys.—Semicond.* **5** 1905 (Engl. Transl.)
[24] Bir G L and Pikus G E 1961 *Fiz. Tverd. Tela* **3** 3050
Bir G L and Pikus G E 1962 *Sov. Phys.—Solid State* **3** 2221 (Engl. Transl.)
[25] Weiler M H 1979 *J. Magn. Magn. Mater.* **11** 131
[26] Luttinger J M 1956 *Phys. Rev.* B **102** 1030
[27] Li X-Z and Xia J-B 2002 *Phys. Rev.* B **66** 115316
[28] *Landolt-Bornstein Group III 17a*
[29] Gel'mont B L, Seisyan R P and Efros Al L 1982 *Fiz. Tekh. Poluprovodn.* **16** 776
Gel'mont B L, Seisyan R P and Efros Al L 1982 *Sov. Phys.—Semicond.* **16** 499 (Engl. Transl.)
[30] Efros Al L and Rosen M 1998 *Phys. Rev.* B **58** 7120
[31] Zutic I, Fabian J and Sarma S D 2004 *Rev. Mod. Phys.* **76** 323